Revision 1

Growth of calcium carbonate in the presence of Se(VI) in silica hydrogel

Ángeles Fernández-González[1,*] and Lurdes Fernández Díaz[2]

Department of Geology. Universidad de Oviedo. 33005 Oviedo, Spain

Department of Crystallography and Mineralogy. Universidad Complutense de Madrid. 28040 Madrid, Spain.

* Department of Geology. Universidad de Oviedo C/ Jesús Arias de Velasco s/n. 33005 Oviedo, Spain. E- mail: mafernan@geol.uniovi.es

ABSTRACT

The effect of Se (VI) on the cystallization of $CaCO_3$ at room temperature was studied using the silica hydrogel method. The $CaCO_3$ crystals obtained were characterized by X-ray powder diffraction, scanning electron microscopy and electron microprobe. The presence of Se(VI) in the growth medium has a clear effect on the polymorph selection of $CaCO_3$, promoting the formation of vaterite and inhibiting that of aragonite. Se(VI) also affects the characteristics of calcite crystals, which show habits progressively more elongated and smaller sizes with increasing Se(VI) concentration in the growth medium. The effect of Se(VI) on both the polymorphic crystallization of $CaCO_3$ and the characteristics of calcite crystals shows features strikingly similar to those of other tetrahedral anionic groups like S(VI) and Cr(VI). This similarity extends to the amount of Se incorporated into the structure of the different $CaCO_3$ polymorphs, with calcite showing Se contents up to 1200 ppm, vaterite up to 500 ppm and aragonite growing

virtually Se-free. The role of Se(VI) on the crystallization of $CaCO_3$ is discussed taking into consideration the physicochemical conditions in the growth medium at nucleation, which were modeled using the PHREEQ code for low-temperature aqueous geochemistry, and the possible effect of the incorporation of the Se(VI) on the relative stability and, by extension, on the solubility of $CaCO_3$ polymorphs.

Keywords: $CaCO_3$ polymorphism, Se (VI), $CaCO_3$ crystallization.

INTRODUCTION

Selenium is regarded as a trace element in the Earth crust, commonly associated with metal-sulfide deposits. Although selenium is an element essential to most organisms, it becomes toxic to life when present in high concentrations (Spallholz 1994; Lemly 2004; Selinus 2005). Human activities such as mining, agriculture, and industrial production of pigments, glasses, electronic devices, etc., have contributed to accelerate the mobilization of selenium, whose concentration in ground waters and soils has undergone a significant increase during the last decades in specific setups (Ong et al. 1997; Ryser et al. 2006). In fact, selenium has recently been identified as a major contaminant in aquatic ecosystems (Lenz and Lens 2008; May et al. 2008). Moreover, this element is also relevant in the context of nuclear waste management due to the high radiotoxicity of its long-lived isotope ^{79}Se (Jörg et al. 2010). According to safety calculations assessments, ^{79}Se is expected to become one of the most contributing isotopes to the global radioactivity, a potential danger existing that high concentrations of ^{79}Se could be released from waste disposals to the biosphere, causing serious long term damage (Olyslaegers et al. 2005; Albrecht and Miquel 2010). The mobility of selenium under earth surface conditions is strongly affected by its tendency to oxidize. Both SeO_3^{2-} and SeO_4^{2-} (hereafter Se(IV) and Se(VI), respectively) are water-soluble (Elrashidi et al. 1987; Masscheleyn et al. 1990). While Se(IV) forms strong bonds with organic matter and oxide and hydroxide mineral surfaces, Se(VI) is not easily adsorbed nor incorporated into solid precipitates. As a result, Se(VI) can rapidly spread both in surface and ground waters (Zhang and Sparks 1990; Balistrieri and Chao 1987; Hayes et al. 1988; Elrashidi et al. 1987). Improving the current knowledge of the Se(VI) capacity to be incorporated into the structure of rock-forming minerals abundant in surface and

sub-surface environments would help to develop efficient strategies to reduce the mobility of this pollutant.

In this work, we study the crystallization of $CaCO_3$ in the presence of Se(VI). The experiments have been conducted using the double diffusion variant of the silica hydrogel method, which reproduces conditions similar to those existing in soils and sediments (Henish et al. 1986; Putnis et al. 1995). Our aim is determining if Se(VI) is incorporated in the $CaCO_3$ crystals in amounts such that could be relevant for the fate of this contaminant in natural environments. Because $CaCO_3$ has several polymorphs whose ability to incorporate Se(VI) can be expected to be different, special attention is paid to the effect of Se(VI) on $CaCO_3$ polymorph selection and to the amount of Se incorporated in each polymorph. Finally, the effect of Se(VI) on $CaCO_3$ crystallization is compared to the effect of Cr(VI), another contaminating ion with similar crystal-chemical characteristics.

EXPERIMENTAL METHODS

Crystal growth and characterization

The crystallization experiments were performed in a double diffusion system. The experimental set-up is shown in figure 1. It consists in a glass U-shaped tube whose two vertical reservoirs are filled with the reactant aqueous solutions, while the horizontal column (18 cm long) is occupied by silica hydrogel (Henish, 1988). The gel was prepared by acidification of a sodium silicate solution (Merck, sp. gr.: 1.509 g/cm^3; pH = 11.2) with 1N HCl to a pH = 5.5. This solution was poured into the horizontal branch of the U-tube prior to polymerization. The silica hydrogel contains ~ 96.5wt% water filling interconnecting micro-sized pores. One of the vertical branches (reservoir A) was filled with 10 cm^3 of a 0.3M $CaCl_2$ aqueous solution and the other branch (reservoir B) was

filled with 10 cm^3 of an aqueous solution with different ratios of Na_2CO_3 and Na_2SeO_4. The simultaneous diffusion of Na_2CO_3 and Na_2SeO_4 from the same reservoir was preferred to the addition of Na_2SeO_4 to the gel during its preparation to avoid possible gel dilution effects. All reagents were analytical grade. The concentration of the parent solutions in the different experiments are compiled in Table1. . The composition of these parent solutions was checked by inductively coupled plasma atomic emission spectroscopy (ICP-AES) with an iCAP 6000 (Thermo) plasma spectrometer.

Upon starting the experiments, reactants diffused from the vertical branches and eventually nucleation and growth occurred by chemical reaction at a defined point within the gel. Crystal growth was monitored by optical microscopy to find the position of the first precipitate in the gel column and the time elapsed between the beginning of the experiment and the observation of the first crystallites under magnification 500x. Henceforth this time will be referred as waiting period (t_W). The experiments were stopped two months after nucleation. Then, the crystals were extracted from the gel by dissolving it in a 1M NaOH solution. The experiments were conducted at 25±0.1 ºC.

Crystals with representative morphologies were selected under a binocular stereomicroscope and studied using scanning electron microscopy in a JEOL 6610-LV microscope, equipped with Energy Dispersive Spectrometer Oxford INCA Energy 350 with X-max50 detector. This scanning electron microscope was also used to observe and analyze central sections of the crystals. Moreover, detailed quantitative analyses of the crystals were obtained by electron microprobe (CAMEBAXSX-100). The identification of the solid phases was carried out by powder X-ray diffraction in a Philips PW1729-1710 diffractometer with graphite monochromator using Cu Kα-radiation.

Modeling of the physicochemical characteristics within the gel

The diffusion of the reactants through the gel leads to the development of concentration gradients which evolve with time and position. Katsikopoulos et al. (2009) stated that the reactant concentration evolution in the column can be described by the one-dimensional algorithm:

$$C(d,t + \Delta t) = mixf \cdot C(d - \Delta t) + (1 - 2 \cdot mixf) \cdot C(d,t) + mixf \cdot C(d + \Delta t) \quad (1)$$

where C is the reactant concentration, d is the distance from the source reservoir, t is the diffusion time and *mixf* is a mixing factor, which depends on the porosity (φ = 1.19), the effective tortuosity of the gel (τ = 0.969), and the diffusion coefficient of the reactant in water (D_w). By combining this algorithm with a speciation model the concentration profiles of the different chemical species in the gel column can be calculated for any diffusion time. In this work concentration profiles were calculated following this protocol and using the multicomponent-diffusion transport tool (MDT) of the geochemical code PHREEQC version 2.18.5570 (Parkhurst and Appelo 2003) and the llnl.dat thermodynamic database.

RESULTS

Nucleation time and location, crystallization sequence and polymorph selection

In the experiments conducted the waiting period for nucleation (t_W) ranged from 468 to 492 hours, with no evident trend relating it to the SeO_4Na_2-CO_3Na_2 concentrations in reservoir B. In all the cases, the first nuclei appeared in a narrow region of the diffusion column (~ 1 cm wide), located around 10 cm from reservoir A. No significant differences regarding the total number of nuclei formed were detected in the different experiments.

After the first nucleation occurred, the length of the gel column occupied by crystals progressively widened, firstly rightwards and leftwards in a second stage. As a result, three crystallization regions could be distinguished in the gel column: Region 1, where the first nuclei formed; Region 2, approximately 6 cm wide and located closer to reservoir B, and Region 3, around 3 cm wide and located closer to reservoir A. The distribution of these regions within the gel column is depicted in Figure 2.

For a given experiment, each region was characterized by specific crystal morphologies and percentages of the three $CaCO_3$ polymorphs, calcite, aragonite and vaterite. The different phases were initially identified using morphological criteria. This identification was subsequently confirmed by X-ray diffraction. The comparison between the results of different experiments evidenced that the presence of Se(VI) strongly affected both the polymorph selection and the crystal morphology. Although in all the experiments calcite always was the predominant $CaCO_3$ polymorph, the amount of vaterite strongly increased with Na_2SeO_4 concentration in reservoir B. This effect was detected in both Region 1 and Region 2, although in a very different extent. Thus, it was extremely marked in Region 2 and very light in Region 1. For example, while no vaterite was detected in any region in experiment E1, where crystallization occurred in the absence of Se(VI), this phase constituted a 56 % of the precipitate in Region 2 in experiment E6, where the initial Na_2SeO_4 concentration in reservoir B was 0.3 M, the highest considered in this work. In contrast, no polymorph other than calcite was found in Region 3 in any experiment. Aragonite crystals were only detected in Region 1. The influence of an increasing initial Na_2SeO_4 concentration in reservoir B on the formation of aragonite in Region 1 seems to match a negative trend, with aragonite representing 15% of the precipitate in E1 (no Na_2SeO_4 in reservoir B), which drops to a 6% in E2 (0.01 M Na_2SeO_4 in reservoir B). A higher increase of the initial Na_2SeO_4 concentration

leads to no significantly higher decrease of the percentage of aragonite formed. These results are summarized in Table 2.

Crystal morphology, size and composition

The crystal morphology of the different $CaCO_3$ polymorphs is differently affected by the presence of SeO_4^{2-} in the crystallization medium. The influence of SeO_4^{2-} concentration on the morphology of both vaterite and aragonite is very limited to null. Thus, vaterite crystals formed in experiments using different initial Na_2SeO_4 concentration showed a limited variety of shapes, which ranged from spheres to aggregates consisting of lens-like individuals (see Fig. 3a,b). Similarly, aragonite appeared as spherulites or sheaf-like aggregates consisting of radiating needle-like crystals, irrespective of the initial Na_2SeO_4 concentration. Fig. 3c shows an example of an aragonite sheaf-like aggregate.

Calcite crystals, on the contrary, showed a wide morphological variability, which correlated with both the location of the crystals within the gel column and the initial Na_2SeO_4 concentration in reservoir B. For Se(VI)-free experiments (E1), calcite always appeared as rhombohedral single crystals. Small differences in shape were observed in crystals formed in the three different regions: The morphology of those crystals which grew in region 1 were hopper or showed poorly developed dendritic branches, slightly differing from the typical rhombohedra. Crystal formed in region 3 were rhombohedra with flat faces bounded by edges which are alternatively sharp, those converging in the three-fold axis, and lobed, those not converging in the three-fold axis. On the other hand, crystals formed in region 2 showed flat $\{10\bar{1}4\}$ surfaces and sharp and well defined edges. Representative examples of these crystals are shown in figure 4.

When calcite grew in the presence of Se(VI), the morphological differences between crystals formed in different regions within the gel column dramatically increased. The

features of calcite crystals formed in regions 1 and 3 coincided fairly well with those of the crystals grown in the same regions in Se(VI)-free experiments: dendritic to hopper crystals in region 1 and rhombohedra with flat faces bounded by edges which are alternatively sharp and lobed in region 3 (Figures 5a, b), and (Figure 5c). In contrast, the morphology of calcite crystals grown in region 2 strongly differed from the typical $\{10\bar{1}4\}$ rombohedron. These crystals were elongated parallel to the c-axis, with rough, rounded surfaces in the prism region, poorly defined $\{10\bar{1}4\}$ and steeper rhombohedron faces and curved edges. Only those edges converging in the tree-fold axis were relatively straight and well defined. Figure 6d-f shows different examples of calcite crystals grown in region 2 in the presence of Se(VI), which are differently elongated and show different development of curved surfaces in the prism region. It is worthwhile to note that significant differences in crystal size have also been observed between the calcite crystals grown both in Se(VI)-free experiments and in regions 1 and 3 in Se(VI)-bearing experiments, whose average sizes were around 1 mm when the experiments were terminated, and calcite crystals grown in region 2 in the presence of Se(VI), whose average size was around 400 μm.

In order to obtain information on the possible incorporation of Se(VI) in the structure of the different $CaCO_3$ polymorphs, a selection of vaterite and aragonite aggregates and calcite single crystals showing different length/width ratios were analyzed using electron microprobe. Very significant differences in the concentration of Se incorporated in the crystals composition were observed between the different polymorphs. Thus, in all the aragonite aggregates studied, Se contents were below the detection limit (100 ppm). Figure 6 shows an example of the Se content profile measured on an aragonite aggregate.

224 On the contrary, Se was detected both in vaterite and calcite. The Se content of vaterite
225 aggregates ranged between 200 and 500 ppm, with a fairly homogenous distribution of
226 Se from core to rim. Examples of Se content profiles in vaterite aggregates are shown in
227 figure 7.
228 Finally, calcite crystals showed a wide variety of Se contents, depending on the region
229 of the gel where they formed. Thus, calcite crystals grown in region 3 showed the
230 lowest Se contents, with Se concentrations that ranged between 200 and 850 ppm and
231 Se being more concentrated in the rim of the crystals. Se contents in crystals grown in
232 region 1 roughly varied between 400 and 650 ppm, with most samples showing a slight
233 Se enrichment in the crystal core. Finally, the highest Se contents were found in the
234 calcite crystals grown in region 2. These crystals showed cores with up to 1200 ppm Se
235 concentration, although Se content rapidly decreases towards the rim. Figure 8 shows
236 representative examples of calcite crystals formed in different regions of the gel column
237 and their Se content profiles.
238
239 **DISCUSSION**
240 **Physicochemical conditions at nucleation**
241 The results of the experiments conducted show that the change in the initial Se(VI)
242 concentration in reservoir B has no effect on the waiting time for nucleation or the first
243 nuclei location in the gel column. In this type of experiments nucleation occurs as a
244 consequence of the chemical reaction between dissolved species counter-diffusing from
245 the reservoirs. At diffusion time = 0, the gel column is chemically homogeneous, but as
246 soon as the experiment starts the counter-diffusion of the reactants leads to the
247 development of concentration gradients that evolve with time and in space. Henish and
248 Garcia-Ruiz (1986a, 1986b) proposed that the location of the first precipitate in counter-

diffusion systems is controlled by the fulfillment of two main conditions: i) The system has to be supersaturated and (ii) the activities of the anions and cations involved in the crystallization have to be similar (equality range condition). These requirements were later experimentally demonstrated (Prieto et al. 1989; 1991; Fernández-González et al. 1999). The actual supersaturation value at the nucleation time and location is determined by the boundary conditions, which in the present case are mainly defined by the length of the diffusion column and the initial concentration of the reactants in the reservoirs. The formation of $CaCO_3$ phases involves the reaction between Ca^{2+} and CO_3^{2-} ions. Since in all the experiments conducted the initial concentrations of $CaCl_2$ and Na_2CO_3 in reservoir A and reservoir B, respectively, were identical and the waiting time for nucleation varied by less than a 5 %, it is to be expected that no significant differences exist in supersaturation at the nucleation time and location. The calculated saturation indexes with respect to the three $CaCO_3$ polymorphs calcite, aragonite and vaterite at nucleation time and location show that this is the case. In all the experiments the system is supersaturated with respect to the three polymorphs, with saturation indexes around 2.7 for calcite, 2.5 for aragonite and 2.1 for vaterite. Figure 9 depicts the distribution of Ca^{2+}, CO_3^{2-} and SeO_4^{2-} concentrations in the gel column at the nucleation time, as modeled using PHREEQC, for experiments E1 and E6. As can be seen, the concentrations of Ca^{2+}, CO_3^{2-} and SeO_4^{2-} are maxima close to the respective reservoirs, progressively decreasing with increasing distance. At the first precipitate location Ca^{2+} and CO_3^{2-} have the same value, i.e. $Ca^{2+}/CO_3^{2-} \approx 1$, thereby fulfilling the reagents activity equality range requirement for nucleation predicted by Henish and García-Ruiz (1986a; 1986b).

As mentioned above, no significant differences in nucleation density were observed in the different experiments. This is consistent with the fact that nucleation occurred at

identical supersaturation in all the cases. It is also worthwhile noting that the pH also was identical, with a value ~ 9.5. Since the SeO_4^{2-}/CO_3^{2-} ratio at nucleation time and location ranged from 0 in experiment E1 to ~ 1.6 in experiment E6, it must be concluded that the presence of Se(VI) in the crystallization medium does not inhibit $CaCO_3$ crystallization by reducing the total number of nuclei formed, at least within the range of Se(VI) concentrations explored.

Polymorph selection

Since in all the experiments conducted nucleation occurred under the identical supersaturations with respect to the different $CaCO_3$ polymorphs, Se(VI) concentration has to be the factor controlling the variation in the ratio of precipitating polymorphs. From our results it can be concluded that Se(VI) promotes the metastable formation of vaterite while inhibiting the nucleation of calcite. This relationship is supported by the fact that vaterite crystals nucleate in the region of the gel column where SeO_4^{2-} concentration is higher as evidenced in Figure 9. The effect of Se(VI) on the formation of aragonite is more complex: the amount of aragonite formed strongly decreases in the presence of a small concentration of Se(VI) but it is not further reduced by an increase in Se(VI) concentration. The promotion of vaterite formation by Se(VI) is in good agreement with previously reported effects of tetrahedral anionic molecules like sulfate and chromate on the crystallization of $CaCO_3$. For example, Fernández-Díaz et al. (2010) studied the temporal evolution of the ratio of $CaCO_3$ polymorphs formed in sulfate-bearing aqueous solutions. These authors reported that higher sulfate contents in the solution lead to higher amounts of vaterite in the precipitate and a progressively more sluggish transformation of vaterite into calcite (Fernández-Díaz 2009, 2010). A direct relationship between dissolved chromate and the amount of vaterite in $CaCO_3$ precipitates has also been reported (Hua et al. 2007; Sánchez-Pastor, 2011a). Moreover,

299 increasing concentrations of chromate progressively retard the transformation of vaterite
300 into calcite (Cruz 2011). Bots et al. (2011) have highlighted that sulfate can play a
301 complex role in $CaCO_3$ polymorphism decreasing the Mg/Ca ratio that switches the
302 polymorph precipitating from seawater from calcite to aragonite. Although carbonate is
303 a triangular planar anionic molecule and large distortions or disruption of local structure
304 would be required to accommodate its substitution by tetrahedral anions, numerous
305 experimental evidences support that sulfate and chromate substitute carbonate in natural
306 and synthetic calcites (Busenberg and Plummer 1985; Frisia et al. 2005; Sánchez-Pastor
307 2011). Moreover, such substitution was concluded from XANES and EXAFS
308 measurementss on calcite single crystals (Staudt et 1994; Tang et al. 2007). Recently,
309 computational modeling showed the viability of a certain degree of carbonate
310 substitution by sulfate in the structure of $CaCO_3$ polymorphs, indicating that this
311 substitution is energetically favorable in vaterite, slightly unfavorable in calcite and very
312 unfavorable in aragonite (Fernández-Díaz et al. 2010). According to this result, the
313 effect of sulfate on the polymorph selection of $CaCO_3$ has been related to a differential
314 solubility behavior of the three $CaCO_3$ polymorphs when they incorporate sulfate. A
315 similar explanation, combined with specific effects on the surface of the different
316 polymorphs has been proposed for the influence of chromate on $CaCO_3$ crystallization
317 (Sánchez-Pastor 2011). In the case of selenate, synchrotron radiation-based studies also
318 provided direct evidence that this anion substitutes carbonate in the structure of calcite
319 (Lamble et al. 1994; Reeder et al. 1994). Selenate is larger than sulfate and almost
320 identical to chromate. From geometrical considerations it can be expected that the
321 incorporation of selenate into $CaCO_3$ polymorphs would be similar to that of chromate
322 but smaller than that of sulfate. Accordingly, the effect of selenate on $CaCO_3$
323 crystallization should be similar to the effect of chromate and less intense than the effect

of sulfate. Indeed, our results confirm that selenate promotes the formation of vaterite in a similar extent as chromate, but not as strongly as sulfate. This is in contrast with the inhibiting effect of selenate on the formation of aragonite, whose nucleation is promoted by chromate and seems to be little affected by sulfate unless in combination with other ions. Understanding the differential effect of tetrahedral anions on aragonite nucleation will require carrying out further research.

Polymorph compositions

The differential incorporation of Se in $CaCO_3$ polymorphs is in good agreement with data in the literature regarding the incorporation of other tetrahedral anionic molecules. For example, it has been reported that while the sulfate content of biogenic aragonite never exceeds 6,000 ppm (Land and Hoops, 1973[39]), it can reach values of several units weight percent in biogenic and inorganic calcites (Busenberg and Plummer 1985). Moreover, the Raman analysis of aragonite grown in silica gel in the presence of chromate showed no vibrational bands which could be assigned to the chromate group. These bands were present both in calcite and vaterite (Sachez-Pastor et al. 2011), showing a higher intensity in calcite. Moreover, microprobe analyses of those calcite crystals yielded Cr contents in the range between 1,500 and 6,000 ppm. These differential incorporation is also in agreement with the conclusion derived from computational modeling that the incorporation of tetrahedral anionic molecules differentially affects the energetics of the different $CaCO_3$ polymorphs (Fernández-Díaz et al 2010), with this incorporation being very unfavorable in the case of aragonite and less so in calcite and vaterite.

The difficulty of the incorporation of Se(VI) into the structure of aragonite could be the basis of the reduction of the amount of aragonite formed in experiments E2 to E6, where crystallization occurs in the presence of Se(VI), in comparison to the amount of

aragonite formed in E1, in the absence of Se(VI). The lower Se content of vaterite crystals in comparison to calcite in region 2 could be explained by the fact that vaterite crystals form earlier. It is worth noting that the evolution of SeO_4^{2-}/CO_3^{2-} ratio is the result of the coupling between mass transfer from the reservoirs and reagent consumption by the growing crystals. It can be assumed that the diffusion of SeO_4^{2-} and CO_3^{2-} will yield no significant differences. Since the consumption of CO_3^{2-} as a result of vaterite crystals is always higher than the consumption of SeO_4^{2-}, the SeO_4^{2-}/CO_3^{2-} ratio will increase as growth proceeds. Therefore, calcite crystals will nucleate in the presence of higher SeO_4^{2-}/CO_3^{2-} ratios than vaterite aggregates.

The Se contents of calcite crystals formed in the different regions correlates well with the Se(VI) concentration in the growth medium as shown Figure 9. SeO_4^{2-} profiles were calculated for the nucleation time and it is not possible to estimate how these profiles evolve along time due to the diffusion disturbance resulting from the growth of the first nuclei. However, these profiles can be used as a reference of the distribution of SeO_4^{2-} concentrations in the gel column. As can be seen, at nucleation time the highest SeO_4^{2-} concentration corresponds to region 2, followed by region 1 and, finally, region 3, with the lowest SeO_4^{2-} concentration, in agreement with the respective Se content of the crystals.

Figure 10 shows the calculated ideal distribution of Ca^{2+}, CO_3^{2-} and SeO_4^{2-} concentrations and the pH in the gel column after 636 hours since the beginning of experiment E6, assuming that no nucleation occurred. This time is 168 hour longer than the actual nucleation time. The ideal profile of SeO_4^{2-} in figure 10 can be considered realistic due to the scarce incorporation of SeO_4^{2-} into crystals formed in region 1. However, since any nucleated crystal represents a sink for Ca^{2+} and CO_3^{2-} ions, ideal profiles for these ions in Figure 10 will significantly differ from the real ones. Indeed,

the consumption of Ca^{2+} and CO_3^{2-} due to the growth of crystals in region 1 will differently disrupt the subsequent evolution of the concentration of these ions in regions 2 and 3. In region 2, closer to reservoir B (CO_3^{2-} source), diffusion disturbances will mainly affect to Ca^{2+} concentration, which will be lower than ideally predicted. On the contrary, in region 3, closer to reservoir A (Ca^{2+} source), a lower concentration than predicted must be expected for CO_3^{2-}. Similarly, because the pH evolution in the gel column is coupled to the concentration of CO_3^{2-}, the characteristics of the pH profile can be considered unrealistic in the gel column from region 1 to reservoir A, where lower values should be expected. $CaCO_3$ crystallization requires high pHs to occur because of the pH-dependent distribution of carbonate species. Therefore, the disruption of CO_3^{2-} diffusion has a stronger influence on the supersaturation profile than that of Ca^{2+}. This can explain that the widening of the length of the gel column occupied by crystals preferentially occurs towards the reservoir B. Moreover, since the incorporation of impurities into crystal structure is favored by high supersaturation levels (Prieto et al. 1997), a lower supersaturation might also explain that almost no SeO_4 is incorporated in the crystals formed in region 3.

Calcite habit evolution

The spatial and temporal evolution of the calcite crystals habit in Se(VI)-free experiments can be explained based on both supersaturation evolution and the specific characteristics of calcite structure (Fernández-González 1999; Fernández-Díaz et al. 2006)). Dendritic crystals in region 1 form first, most likely under higher supersaturation. The reagent consumption due to the growth of crystals in region 1 determines that the nucleation and growth of crystals in region 2 and 3 occurs at progressively lower supersaturations. As a result, the predominant growth mechanism evolves from adhesive to two-dimensional nucleation and, finally, spiral growth,

399 explaining the parallel evolution from dendritic morphologies to hopper crystals and
400 well developed rombohedra. It is worthwhile noting that calcite dendritic and hopper
401 crystals are characterized by a more or less marked cleft in their equatorial region,
402 which results from a different development of the edges converging in the three-fold
403 axis in comparison to those non-converging (Figure 4a,b). All these edges are parallel to
404 the $\langle\bar{4}41\rangle$ PBC (Heijnen, 1985). However, due to the orientation of the carbonate
405 groups in calcite structure determines that parallel growth step edges that advance in
406 opposite directions contain growth sites with non-equivalent geometries (Paquette and
407 Reeder, 1995; Reeder and Rakovan, 1999; Staudt et al. 1994). This non-equivalence
408 determines that, as has extensively been evidenced by molecular scale observations
409 (Astilleros et al. 2006; Hillner et al. 1992; Jordan and Rammensee, 1998; Teng et al.
410 2000), opposing steps advance at very different rates, which in turn can explained the
411 different development of parallel edges bounding $\{10\bar{1}4\}$ faces in calcite (Fernández-
412 Díaz et al. 2006).
413 A similar combination of the supersaturation change and the specific characteristics of
414 the $\langle\bar{4}41\rangle$ edges can give account of the morphological evolution of calcite crystals
415 formed in Se(VI)-bearing gels in regions 1 and 3 and can also explain the alternation of
416 sharp and lobbed edges bounding $\{10\bar{1}4\}$ faces and the marked equatorial cleft shown
417 by crystals formed in region 2. However, these crystals are progressively more
418 elongated along the *c* axis due to the development of curved surfaces in the prism region
419 as the concentration of Se(VI) in reservoir B increases. This characteristic is also shown
420 by crystals formed in the presence of other tetrahedral anions like SO_4^{2-}, CrO_4^{2-} or
421 HPO_4^{2-} (Fernández-Díaz 2010; Sánchez-Pastor 2011; Suzuki 1986), whose effect on

422 calcite habit has been related to selective binding on sites in prism surfaces (Parker et al.
423 1993; Titiloye et al. 1993).
424

425 ## CONCLUSIONS

426 The experiments presented in this work show that the presence of Se (VI) influences the
427 crystallization of calcium carbonate precipitated from aqueous solutions. The
428 incorporation of selenate in the $CaCO_3$ crystals is limited, but it affects both the stability
429 of the different $CaCO_3$ polymorphs and the morphology and size of the calcite crystals.
430 Specifically, the presence of Se (VI) seems to promote the stabilization of vaterite and
431 tends to inhibit the nucleation of aragonite. The tetrahedral anion SeO_4^{2-} can be
432 incorporated in the structure of calcite and vaterite when they precipitate far from
433 equilibrium, but it was not observed in aragonite grown under identically high
434 supersaturation conditions. The modification of the solubility of the impure phases with
435 respect to pure calcite and vaterite might explain the effect of selenate on the
436 polymorphism of $CaCO_3$. Calcite crystals grown from aqueous solutions in the presence
437 of Se (VI), tend to develop elongated morphologies and their sizes are found to be
438 smaller when the selenium concentration is higher.
439

440 **Acknowledgement**

441 This research was supported by MICINN-Spain, under grants CGL2010-20134-C02-01
442 and CGL2010-20134-C02-02 and by the German Federal Ministry of Education and
443 Research (ImmoRad: Basic research on Immobilization of long-lived Radionuclides by
444 interaction with relevant secondary repository-phases).
445
446

References

Albrecht, A., and Miquel, S. (2010) Extension of sensitivity and uncertainty analysis for long term dose assessment of high level nuclear waste disposal sites to uncertainties in the human behavior. Journal of Radioactivity, 101, 55-67.

Armbruster, M. (2008) An evaluation of selenium concentrations in water, sediment, invertebrates, and fish from the Solomon River Basin. Environmental Monitoring and Assessment, 137, 213–232.

Astilleros, J.M., Pina, C.M., Fernández-Díaz, L., and Putnis, A. (2006) Nanoscale phenomena during the growth of solid solutions on calcite $\{10\bar{1}4\}$. Chemical Geology, 225, 322-335.

Balistrieri, L.S., and Chao, T.T. (1987) Selenium adsorption by goethite: Soil Science Society of America Journal, 51, 1145‐1151

Cruz, J., Sánchez-Pastor, N., Gigler, A.M., and Fernández-Díaz, L. (2011) Vaterite ($CaCO_3$) Stability in the Presence of Chromate. Spectroscopy Letters, 44, 495-499.

Bots, P., Benning, L.G., Rickaby, R.E.M., and Shaw, S. (2011) The role of SO_4 in the switch from calcite to aragonite seas. Geology, 39, 331–334.

Busenberg, E., and Plummer, N. (1985) Kinetic and thermodynamic factors controlling the distribution of SO_3^{2-} and Na^+ in calcites and selected aragonites. Geochimica et Cosmochimica Acta, 49, 713–725.

Elrashidi, M.A., Adriano, D.C., Workman, S.M., and Lindsay, W.L. (1987) Chemical-equilibria of selenium in soils – a theoretical development. Soil Science, 144, 141–152.

Fernández-Díaz, L., Astilleros J.M., and Pina. C.M (2006) The morphology of calcite crystals grown in a porous medium doped with divalent cations. Chemical Geology, 225, 314-321.

Fernández-Díaz, L., Fernández-González, A., and Prieto, M. (2010) The role of sulfate groups in controlling $CaCO_3$ polymorphism. Geochimica et Cosmochimica Acta. 74, 6064-6076.

Fernández-Díaz, L., Pina, C.M., Astilleros, J.M., and Sánchez-Pastor, N. (2009) The carbonation of gypsum: Pathways and pseudomorph formation. American Mineralogist 94, 1223-1234.

Fernández-González, A., Prieto, M., Putnis, A., and López-Andrés, S. (1999) Concentric zoning patterns in crystallizing $(Cd,Ca)CO_3$ solid solutions from aqueous solutions. Mineralogical Magazine, 63, 331-343.

Frisia, S., Borsato, A., Fairchild, I.J., and Susini, J. (2005) Variations in atmospheric sulphate recorded in stalagmites by synchrotron mirco-XRF and XANES analyses. Earth and Planetary Science Letters, 235, 729-740.

Hayes, K.F., Papelis, C., and Leckie, J.O. (1988) Modelling ionic strength effects on anion adsorption at hydrous oxide/solution interfaces. Journal of Colloid and Interface Science, 125, 717–726.

Heijnen, W.M.M. (1985) The morphology of gel grown calcite. Neues. Jahrbuch für Mineralogie. Monatshefte, 8, 357-362.

Henisch, H.K. (1988) Crystals in Gels and Liesegang Rings. Cambridge University Press, Cambridge.

Henish, H.K., and Garcia·Ruiz J.M. (1986a) Crystal growth in gels and Liesegang ring formation. I Diffusion relationships. Journal of Crystal Growth, 75, 195-202.

Henish, H.K., and Garcia·Ruiz J.M. (1986b) Crystal growth in gels and Liesegang ring formation. II Crystallization criteria and succesive prccipitation. Crystal Growth, 75, 203-211.

Hillner, P.E., Gratz, A.J., Manne, S., Hansma, P.K. (1992) Atomic-scale imaging of calcite growth and dissolution in real time. Geology 20, 359-362.

Hua, B., Deng, B. L., Thorton, E. C., Yang, J., and Amonette, J.E. (2007) Incorporation of chromate into calcite structure during coprecipitation. Water, Air & Soil Pollution, 179, 381-390.

Jordan, G., Rammensee, W. (1998) Dissolution rates of calcite (10 4) surfaces obtained by scanning force microscopy: microtopography-based dissolution kinetics on surfaces with anisotropic velocities. Geochimica et Cosmochimica Acta, 62, 941-947.

Jörg, G., Bühnemann, R., Hollas, S., Kivel, N., Kossert, K., Van Winckel, S., and Gostomski, C.L. (2010) Preparation of radiochemically pure 79Se and highly precise determination of its half-life. Applied Radiation and Isotopes, 68, 2339-2351.

Katsikopoulos, D., Fernández-González, A., and Prieto, M. (2009) Crystallization behaviour of the (Mn,Ca)CO_3 solid solution in silica gel: nucleation, growth and zoning phenomena. Mineralogical Magazine, 73, 269-284.

Lamble, G.M., Lee, J.F., Staudt, W.J., and Reeder R.J. (1995) Structural studies of selenate incorporation into calcite crystals. Physica B, 208-209, 589-590.

Lemly, A.D. (2004) Aquatic selenium pollution is a global environmental safety issue. Ecotoxicology and Environmental Safety, 9, 44–56.

Lenz, M., and Lens, P.N.L. (2008) The essential toxin: the changing perception of selenium in environmental sciences. Science of The Total Environment, 407, 3620–3633.

520 Masscheleyn, P.H., Delaune, R.D., and Patrick W.H (1990) Transformations of
521 selenium as affected by sediment oxidation reduction potential and pH.
522 Environmental Science and Technology, 24, 91–96.
523 Möller, G. (2006) Microscopically focused synchrotron X-ray investigation of selenium
524 speciation in soils developing on reclaimed mine lands. Environmental Science
525 and Technology, 40, 462-467.
526 Olyslaegers, G., Zeevaert, T., Pinedo, P., Simon, I., Prohl, G., Kowe, R., Chen, Q.,
527 Mobbs, S., Bergstrom, U., Hallberg, B., Katona, T., Eged, K., and Kanyar, B.
528 (2005) A comparative radiological assessment of five European biosphere systems
529 in the context of potential contamination of well water from the hypothetical
530 disposal of radioactive waste. Journal of Radiological Protection, 25, 375–391.
531 Ong, C.G., Herber M.J., Dahlagren, R.A., and Tanji, K.K. (1997) Trace Elements (Se,
532 As, Mo, B) contamination of evaporates in hypersaline agricultural evaporation
533 ponds. Environmental Science and Technology, 31, 831-836.
534 Paquette, J., Reeder, R.J., (1995) Relationships between surface structure, growth
535 mechanism, and trace element incorporation in calcite. Geochimica et
536 Cosmochimica Acta 59, 735-749.
537 Parker, S.C., Titiloye, J.O., Watson, G.W. (1993) Molecular Modelling of Carbonate
538 Minerals: Studies of growth and morphology, Philosophical Transactions of the
539 Royal Society of London A, 344, 37-48.
540 Parkhurst, D.L., and Appelo, C.A.J. (2003) In: User's guide to PHREEQC (Version 2):
541 A computer program for Speciation, Batch-Reaction, One-Dimensional Transport
542 and Inverse Geochemical Calculations. U.S. Geological Survey Water Resources
543 Investigations Report, Washington D.C.

Prieto, M., Fernández-Díaz, L., and López-Andrés, S. (1989). Supersaturation evolution and first precipitate location in crystal growth in gels; Aplication to barium and strontium carbonates. Journal of Crystal Growth, 98, 447-460.

Prieto, M., Fernández-Díaz, L., and López-Andrés, S. (1991) Spatial and evolutionary aspects of nucleation in diffusing- reacting systems. Journal of Crystal Growth, 108, 770-778.

Prieto, M., Fernández-González, A., Putnis, A., and Fernández-Díaz, L. (1997) Nucleation, growth, and zoning phenomena in crystallizing $(Ba,Sr)CO_3$, $Ba(SO_4,CrO_4)$, $(Ba,Sr)SO_4$, and $(Cd,Ca)CO_3$ solid solutions from aqueous solutions. Geochimica et Cosmochimica Acta, 61, 3383-3397.

Putnis, A., Prieto, M., and Fernández-Díaz, L. (1995) Fluid supersaturation and crystallization in porous media. Geological Magazine, 132, 1-13.

Reeder, R:J., Lamble G., Lee, J.F. and Staudt, W. (1994) Mechanism of SeO42- substitution in calcite: An XAFS study. Geochimica et Cosmochimica Acta 58, 5639-5646.

Reeder, R.J., Rakovan, J. (1999) Surface structural controls on trace element incorporation during crystal growth. In: B. Jamtveit and P. Meakin, Eds., Growth, Dissolution and Pattern Formation in Geosystems. Kluwer Academic Publishers.

Ryser, A.L., Strawn, D.G., Marcus, M.A., Fakra, S., Johnson-Maynard, J.L., and Möller, G. (2006) Microscopically focused synchrotron X-ray investigation of the speciation in soils developing on reclaimed mine lands. Environmental Science and Technology, 40, 462-467.

Sánchez-Pastor, N., Gigler, A.M., Cruz, J.A., Park, S.H., Jordan, G., and Fernández-Díaz, L. (2011) Growth of calcium carbonate in the presence of Cr(VI). Crystal Growth and Design, 11, 3081–3089.

569 Selinus, O. (Ed.) (2005) Essentials of Medical Geology. Elsevier Academic Press,
570 London.
571 Spallholz, J.E. (1994) On the nature of selenium toxicity and carcinostatic activity.
572 Biology and Medicine, 17, 45-64.
573 Staudt, W.J., Reeder, R.J. and Schoonen, W.A.A. (1994) Surface structural controls on
574 compositional zoning of SO_4^{2-} and SeO_4^{2-} in synthetic calcite single crystals.
575 Geochimica et Cosmochimica Acta, 58, 2087-2098
576 Suzuki, T., Inomata, S., and Sawada, K. (1986) Adsorption of phosphate on calcite.
577 Journal of the Chemical Society, Faraday Transactions, 82, 1733-1743.
578 Tang, Y., Elzinga, E.J., Lee, Y.J, and Reeder, R.J. (2007) Coprecipitation of chromate
579 with calcite: Batch experiments and X-ray absorption spectroscopy. Geochimica
580 et Cosmochimica Acta, 71, 1480–1493.
581 Teng, H., Dove, P.M. and De Yoreo, J.J. (2000) Kinetics of calcite growth: Surface
582 processes and relationships to macroscopic rate laws, Geochimica et
583 Cosmochimica Acta, 64, 2255-2266.
584 Titiloye, J.O., Parker, S.C.; Mann, S. (1993) Atomistic Simulation of Calcite Surfaces
585 and the Influence of Growth Additives on their Morphology, Journal of Crystal
586 Growth, 131, 533-545.
587 Zhang, P., and Sparks D.L. (1990) Kinetics of Selenate and Selenite
588 Adsorption/Desorption at the Goethite/Water Interface. Environmental Science
589 and Technology, 24, 1848-1856.
590

Figure captions

Figure 1: Experimental set-up used for crystal growth

Figure 2: Se-content content in the calcite analyzed by electron microprobe (a, c, b). The dotted grey line on plots represents the detection limits in the Se-analysis. The analyses were carried out on central polished sections of the shown crystals (b, d, f). Crystal b grew in Region 2, crystal c in Region 1 and crystal f in Region 3.

Figure 3. Distribution of crystallization regions in the gel column.

Figure 4: Morphologies of vaterite (a,b) and aragonite (c) grown in silica gel in the presence of Se (VI).

Figure 5: Morphologies of calcite observed for Se(VI)-free experiments in the different regions (r) of the gel column.

Figure 6: Morphologies of calcite grown in silica gel in the presence of Se (VI). The experiments in which the crystals were obtained (E) and the corresponding gel column regions (r) are indicated in each photo. The presence of Se (VI) in the aqueous solution increases form 6a to 6f.

Figure 7: Se-content (a) determined by electronic microprobe analysis carried out on a central section of an aragonite aggregate (b). The dotted grey line on plot a represents the detection limits in the Se-analysis.

Figure 8: Se-content in vaterite determined by microprobe analysis (a, c). The dotted grey line on plots represents the detection limits in the Se-analysis. The analyses were carried out on central polished sections of the aggregates (b, d).

Figure 9. Activity for Ca^{2+} (dotted line), CO_3^{2-} (solid line) and SeO_4^{2-} (dashed line) and pH profile at nucleation time as modeled using PHREEQC for experiments E1 (a,c) and E6 (b,d).

615 Figure 10. (a) Activity for Ca^{2+} (dotted line), CO_3^{2-} (solid line) and SeO_4^{2-}
616 (dashed line) and (b) pH profiles as modeled using PHREEQC for experiment E6
617 considering 636 hours diffusion time and no disruption of the diffusion progress due to
618 crystallyzation.

619

620
621

622
623 Table 1: Initial concentration of the parent solutions.

Experiment	Parent solutions		
	Reservoir A	Reservoir B	
	$CaCl_2$ (M ±0.005)	Na_2CO_3 (M ±0.005)	Na_2SeO_4 (M ±0.005)
E1	0.3	0.3	0.0
E2	0.3	0.3	0.01
E3	0.3	0.3	0.03
E4	0.3	0.3	0.05
E5	0.3	0.3	0.1
E6	0.3	0.3	0.3

624
625

626

627
628 Table 2. Percentages of calcite, vaterite and aragonite (C, V, A) in the different regions
629 of the U-tube. The last three columns show the percentages in the entire tube. The
630 percentage of calcite, aragonite and vaterite was estimated by counting all the crystals
631 inside the U-tube of each polymorph (identified with morphological criteria) under the
632 binocular stereomicroscope at the end of each experiment, immediately before their
633 extraction. The average number of crystals obtained in the experiments was ~ 200.

Experiment	Region 1			Region 2			Region 3			Total		
	C	V	A	C	V	A	C	V	A	C	V	A
E1	85	-	15	100	-	-	100	-	-	94	-	6
E2	94	-	6	84	16	-	100	-	-	85	8	2
E3	94	-	6	77	23	-	100	-	-	84	9	2
E4	93	1	6	70	30	-	100	-	-	80	18	2
E5	94	1	5	58	42	-	100	-	-	73	25	2
E6	93	2	5	44	56	-	100	-	-	60	38	2

634
635

636
637

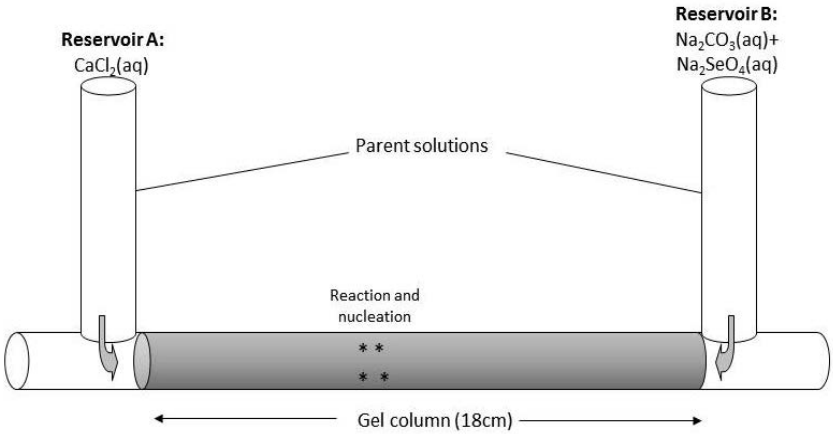

638

639 Figure 1: Experimental set-up used for crystal growth

640

641

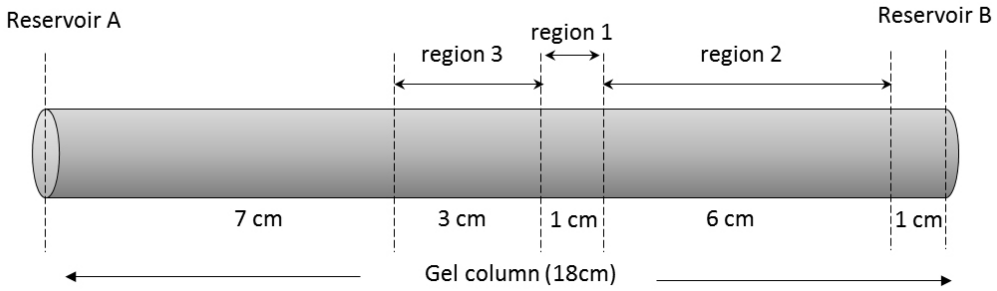

642

643 Figure 2. Distribution of crystallization regions in the gel column.

644

645

646

647 Figure 3: Morphologies of vaterite (a,b) and aragonite (c) grown in silica gel in the

648 presence of Se (VI).

649

650

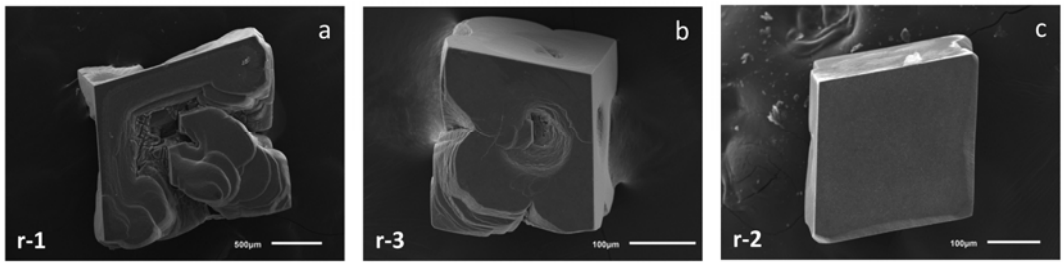

651

652 Figure 4: Morphologies of calcite observed for Se(VI)-free experiments in the

653 different regions (r) of the gel column.

654

655

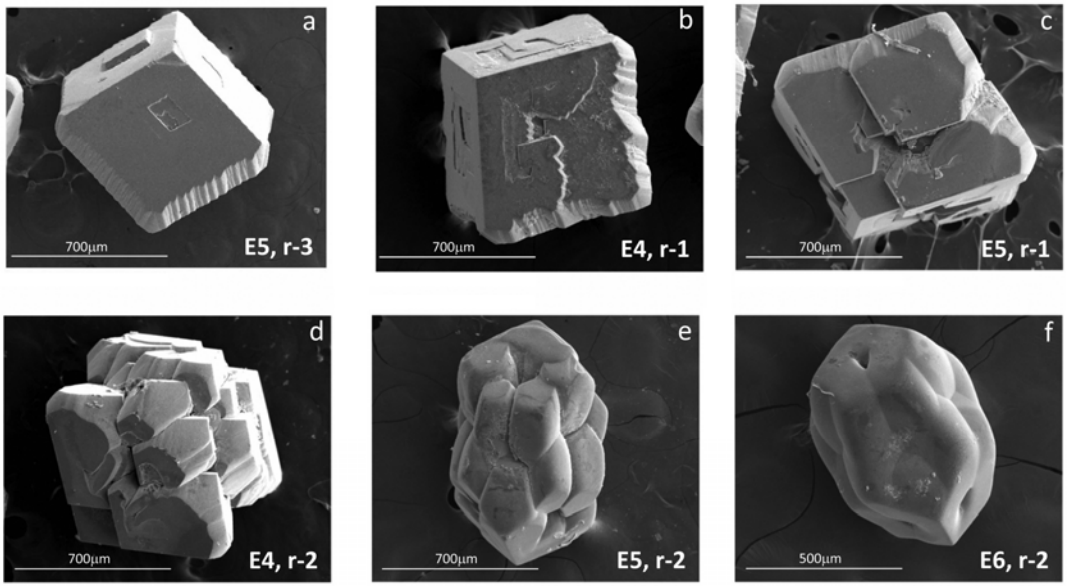

656

657 Figure 5: Morphologies of calcite grown in silica gel in the presence of Se (VI). The
658 experiments in which the crystals were obtained (E) and the corresponding gel column
659 regions (r) are indicated in each photo. The amount of Se (VI) in the aqueous solution
660 increases form 6a to 6f.

661

662

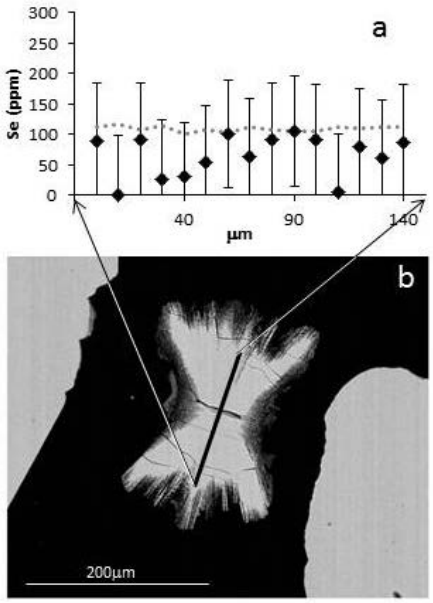

663

664 Figure 6: Se-content (a) determined by electronic microprobe analysis carried out on a
665 central section of an aragonite aggregate (b). The dotted grey line on plot a represents
666 the detection limits in the Se-analysis.

667

668

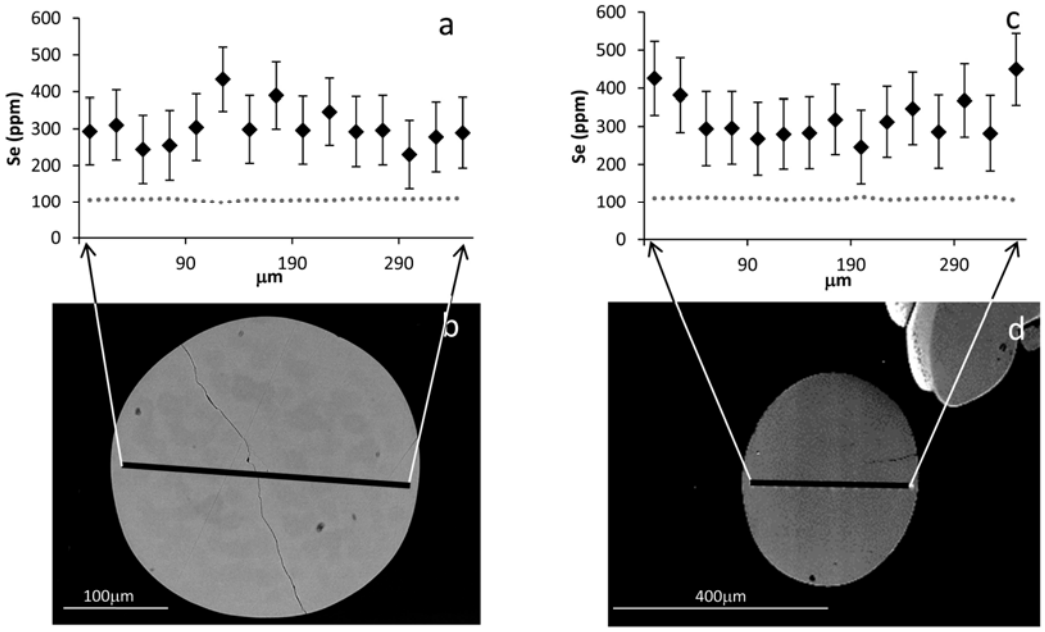

669

670

671

672 Figure 7: Se-content in vaterite determined by microprobe analysis (a, c). The dotted
673 grey line on plots represents the detection limits in the Se-analysis. The analyses were
674 carried out on central polished sections of the aggregates (b, d).

675

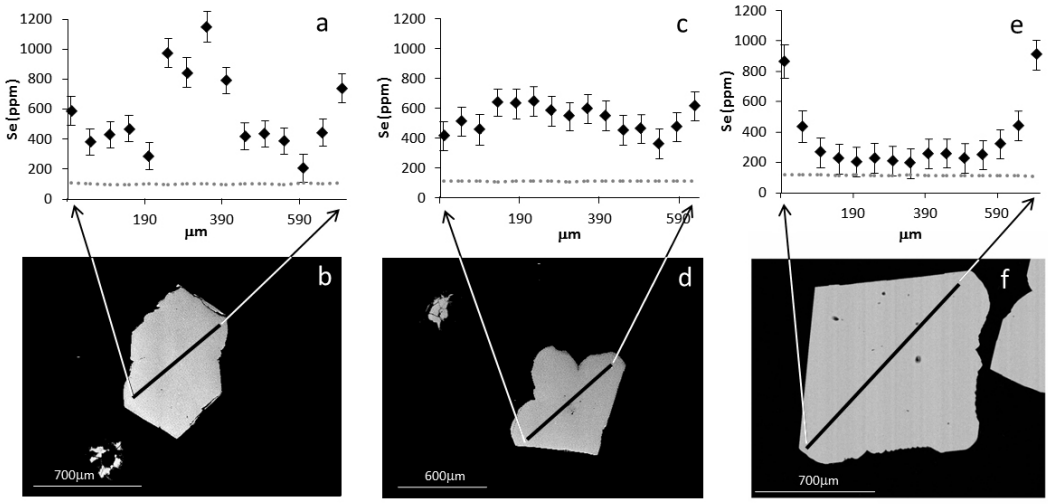

Figure 8: Se-content content in the calcite analyzed by electron microprobe (a, c, b). The dotted grey line on plots represents the detection limits in the Se-analysis. The analyses were carried out on central polished sections of the shown crystals (b, d, f). Crystal b grew in region 2, crystal c in region 1 and crystal f in region 3.

695

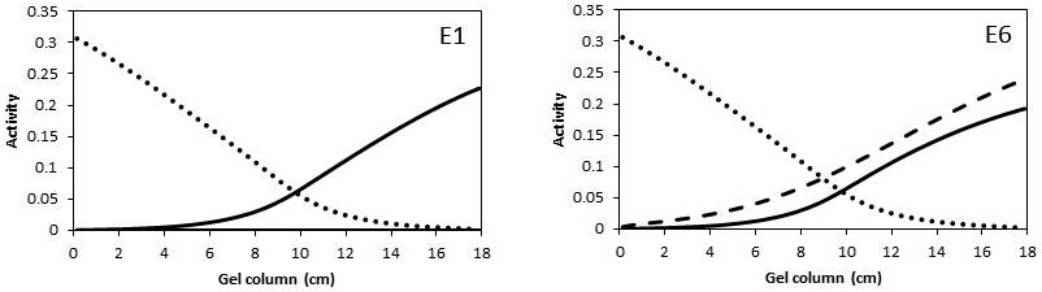

696

697 Figure 9. Activity profiles at nucleation time for Ca^{2+} (dotted line), CO_3^{2-} (solid line)

698 and SeO_4^{2-} (dashed line) as modeled using PHREEQC for experiments E1 and E6.

699